JOURNAL OF MATERIALS SCIENCE 10 (1975) 1105–1118

Hydrostatic extrusion of solid polymers

Part 5 *Structure and molecular orientation of extruded polyethylene*

KAZUO NAKAYAMA, HISAAKI KANETSUNA
Research Institute for Polymers and Textiles, Sawatari 4, Kanagawa-ku, Yokohama 221, Japan

The hydrostatic extrusion of high density polyethylene rod was studied over a wide range of temperatures. The extrudates had smooth surfaces. Those with high extrusion ratios possessed unusual properties being highly transparent and fibrous. The molecular orientation and structural changes due to the hydrostatic extrusion were investigated using wide- and small-angle X-ray diffraction techniques and birefringence. The partial transformation from the orthorhombic to the monoclinic structure occurred in the extrudate obtained at low temperatures (especially at room temperatures). The small-angle X-ray scattering pattern of extrudate for low extrusion ratio showed a diagram with six intensity maxima. On the other hand, for the high extrusion ratio, a diagram with two meridional intensity maxima elongated perpendicular to meridian was observed. At the extrusion ratio $R_E \geqslant 6$, the chain axes of polyethylene became aligned to the extrusion direction. Small-angle X-ray scattering patterns showed that the new fibre structure began to appear at an extrusion ratio as low as $R'_E = 3.0$. The structure of the extrudate at a high extrusion ratio was accounted for by the highly-oriented fibre structure consisting of stacks of folded chain crystallites and the interfibrillar amorphous chain bundles.

1. Introduction

Hydrostatic extrusion, adapted from metal working, in which a polymer rod is extruded into a finished form without heating to the molten state has recently become a subject of great interest. Experiments on the hydrostatic extrusion of a range of difficult materials, including a few polymers, have been described by Pugh and Low [1]. Several investigators [2-4] reported the processing of polymers, e.g. polyethylene, polypropylene and poly(vinyl chloride) etc. Recently, Williams studied the tensile and torsional moduli of the hydrostatically-extruded polypropylene [5].

The structural changes of polyethylene accompanied by different modes of deformation (e.g. stretching, rolling and compression) have been investigated by Hay and Keller [6], Meinel *et al.* [7], and many other authors. Imada *et al.* [8] reported in detail experiments of direct extrusion of solid polyethylene.

In the previous papers of this series [9-11], the effects of extruding conditions on the deformation of high-density polyethylene rods were studied. The main points of the results may be briefly summarized as follows:

(1) Extrusion pressure – displacement curves could be classified into three groups: (a) the steady-state extrusion; (b) the presence of initial peak in the curve; (c) the occurrence of the "stick-slip" phenomenon.

(2) Highly oriented extrudates with smooth surface were obtained by the steady-state extrusion.

(3) For the extrusion at lower temperature with use of a large angle die, the "stick-slip" phenomenon was observed. The "stick-slip" caused fluctuations of diameter of the extrudate along its length or generated cracks in it.

(4) The minimum pressure required for extrusion (P_0) decreased with the increase of the temperature of extrusion.

(5) In the hydrostatic extrusion of polyethylene the pressure medium acts as lubricant.

Hydrostatic extrusion can convert the polymer rod into a finished form having a desired

Part 4: Structural change of polyacetal resin in hydrostatic extrusion, *J. Japan Soc. Tech. Plasticity* **15** (1974) 744.

diameter. The product having a homogeneous cross-section along its length can be obtained by means of the hydrostatic extrusion of polyethylene over the temperature range 20 to 110°C. At the same time the molecular orientation is introduced into it. The hydrostatic extrusion is, therefore, of importance in the practical use of materials and is very convenient for the study of the plastic deformation of polyethylene. The purpose of the present paper is to determine the effects of extrusion temperature and extrusion ratio on the molecular orientation of the crystalline and amorphous regions of polyethylene.

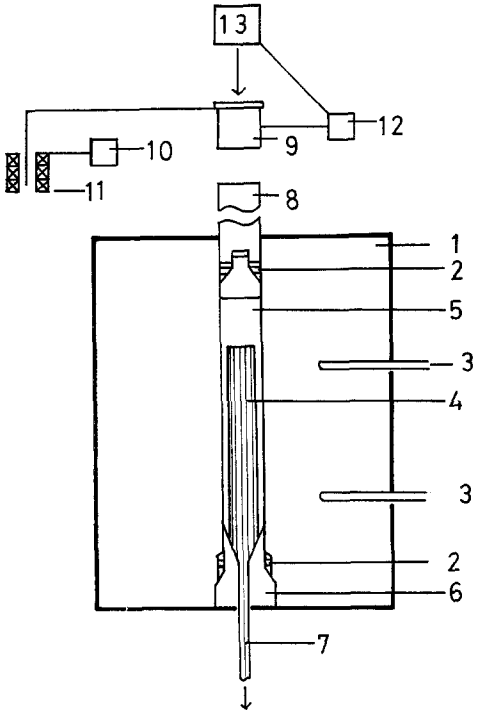

Figure 1 General view of the hydrostatic extrusion apparatus. 1. High pressure container, 2. high pressure seals, 3. thermocouple, 4. cylindrical billet, 5. pressurized fluid, 6. extrusion die, 7. extruded product, 8. plunger, 9. load cell, 10. recorder, 11. displacement meter, 12. recorder, 13. pressure control apparatus.

2. Experimental

2.1. Hydrostatic extrusion

The general view of the apparatus for hydrostatic extrusion is schematically drawn in Fig. 1. The high pressure container (especially manufactured by Kobe Steel Ltd), which can be used at pressures up to 10 000 kg cm^{-2} with a billet (polymer rod) 7 mm in diameter, consists of an extrusion cylinder, die and piston head. The container can be heated with a ribbon heater wound round it and the temperature may be controlled with a PID-SCR regulator.

The commercial rods of high density polyethylene Hizex* 5100B (M.I. = 0.25, $\bar{M}_v = 8.5 \times 10^4$) were used as the starting materials. The solid cylindrical billet (diameters 4.3_7, 5.0_5 and 6.0 mm), with a nose machined on one head, was fitted into the conical entry of the die. The container was then filled with the high pressure medium, glycerin, and the piston head with high pressure seals was inserted. Loading was carried out using a tensile testing machine Tensilon (Toyo Baldwin Co, Ltd, UTM-1-5 ton) capable of giving a constant load on the plunger during the extrusion. The extrusion pressure, i.e. fluid pressure, was estimated from the test machine load and the piston cross-sectional area, where a redundant load due to the friction between the cylinder and the high pressure seals on the piston head was corrected.

In general, there is an optimum die angle at which the extrusion pressure is minimum for a given extrusion ratio[1, 12]. In fact, the optimum die angle ($2\alpha_{opt}$) for the hydrostatic extrusion of polyethylene was 50 to 60° [11]. When the extrusion of polyethylene was carried out through a small-angle die (semi-cone angle α, 10°) at a constant pressure, a highly oriented product with an excellent smooth surface was obtained [9]. Therefore, in this paper dies with small entrance angles (semi-cone angle α, 10°) were used exclusively. Dies have a throat of 2.0 and 2.5 mm diameter and of 10 mm length. Their clearance angle is 5°.

The extrusion ratio (R_E) is defined as the ratio of the cross-sectional area before and after extrusion, and is expressed as $(D_b/D_e)^2$, where D_b and D_e are the diameter of billet and extruded product, respectively. If one assumes that the deformation takes place without any appreciable change of volume, R_E corresponds to the draw ratio. For convenience, the extrusion ratio $R'_E = (D_b/D_d)^2$ was also used, where D_d was the diameter of die aperture. Here, R'_E is the "tool standard" extrusion ratio and this is not always equal to R_E owing to the elastic recovery of products and/or the so-called spring-back.

Fig. 2 shows the pressure required for extrusion of a polyethylene rod at various tempera-

*Trademark, Mitsui Petrochemical Co Ltd.

tures. The figure shows the pressure at which the extruded product with a smooth surface was obtained satisfactorily with extrusion ratios ranging from 3.0 to 9.0.

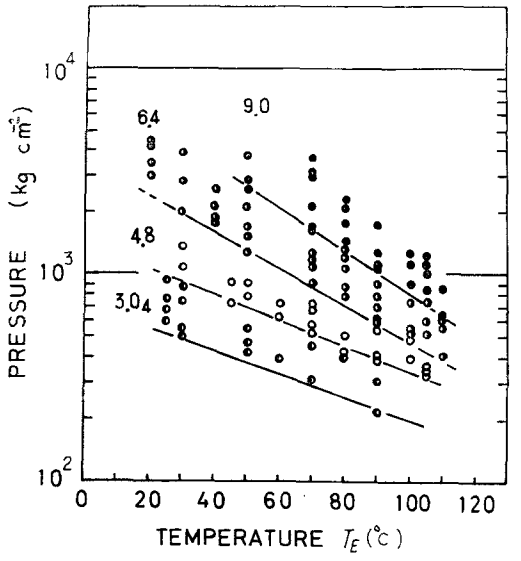

Figure 2 Extrusion pressure at various temperatures in the hydrostatic extrusion of commercial polyethylene rod. The straight lines show the relationships between the minimum pressure required for extrusion and the extrusion temperature. Satisfactory extrusion obtained at extrusion ratio (R'_E), ◐: 3.0, ○: 4.8, ◑: 6.4, ●: 9.0 (from [10]).

2.2. X-ray diffraction

Wide-angle X-ray diffraction patterns were taken with a flat camera. Ni-filtered Cu$K\alpha$ radiation (35 kV, 15 mA) was used. Small-angle X-ray scattering patterns were taken with a vacuum camera (Rigaku-Denki), where the specimen to film distance was 300 mm and the beam stop was 1.5 mm diameter. Ni-filtered Cu$K\alpha$ radiation (50 kV, 90 mA) by means of Rota Unit RU-3SH (Rigaku-Denki), and pin-hole collimators, 0.3 and 0.2 mm diameter, were used.

For some specimens, wide-angle radial scans were made. Ni-filtered Cu$K\alpha$ radiation was used and the scattering radiation was detected by a scintillation counter in conjunction with a pulse height analyser.

The degree of crystalline c-axis orientation (f_c) was evaluated by using Hermans' type orientation function [13]. For this purpose, azimuthal scannings of (200) and (020) reflections were carried out with a Geiger Flex (Rigaku-Denki) from which $\langle\cos^2\phi_{200}\rangle$ and $\langle\cos^2\phi_{020}\rangle$ were evaluated by general procedure. The degree of a-, b- and c-axis orientation were expressed by f_a, f_b and f_c, respectively.

$$f_a = \tfrac{1}{2}(3\langle\cos^2\phi_{200}\rangle - 1) \quad (1)$$

$$f_b = \tfrac{1}{2}(3\langle\cos^2\phi_{020}\rangle - 1) \quad (2)$$

$$f_c = -(f_a + f_b) \quad (3)$$

2.3. Density

Density (d) was measured by the density gradient column method in a mixture of ethanol and water at 25°C. The density distribution in the column was determined by use of caliburated glass beads. Crystalline fraction in volume (X_v) was calculated as follows:

$$d = d_c X_v + d_a(1 - X_v) \quad (4)$$

Here, 1.00_8 and 0.855 g cm^{-3} were taken for the crystalline density (d_c) and the amorphous density (d_a), respectively [14].

2.4. Birefringence

Birefringence (Δn) was measured by means of retardation method under a polarizing microscope. A sodium lamp was used as a light source. The birefringence gives the overall orientation.

2.5. Degree of amorphous orientation

The degree of amorphous orientation (f_{am}) was estimated from the following expressions:

$$\Delta n = \Delta n_c X_v + \Delta n_{am}(1 - X_v) \quad (6)$$

$$\Delta n_c = \Delta n_c^{\circ} f_{am} \quad (7)$$

$$\Delta n_{am} = \Delta n_{am}^{\circ} f_{am} \quad (8$$

where Δn_c° and Δn_{am}° are the intrinsic birefringence values of the ideally oriented crystalline and amorphous regions, respectively. Here, $\Delta n_c^{\circ} = 0.0572$ [15] and $\Delta n_{am}^{\circ} = \Delta n_c^{\circ} . d_a/d_c = 0.0485$ were used. In Equation 6 the possibility of "form birefringence" [21] was neglected.

3. Result and discussion

3.1. Partial transformation from orthorhombic to monoclinic structure

The wide-angle X-ray diffraction pattern of the starting material (PE rod) showed the random crystalline orientation. Since the hydrostatic extrusion gives rise to the plastic deformation of polyethylene, changes in molecular orientation and in the texture must occur. Figs. 3a and 4a

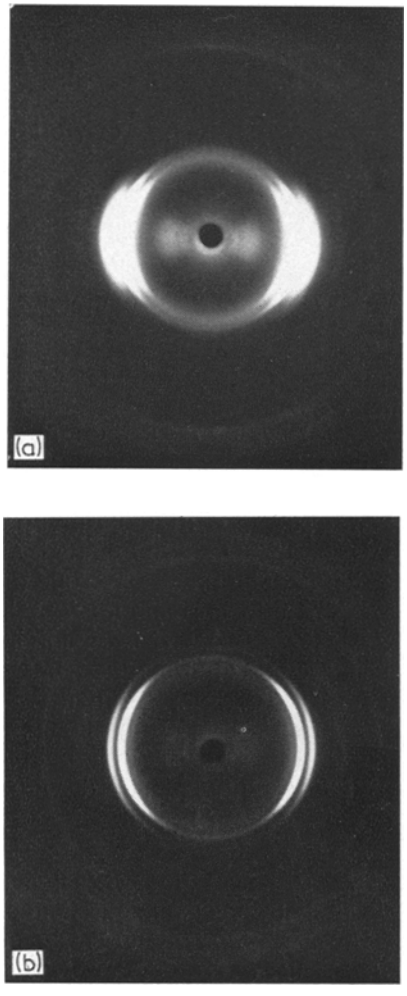

Figure 3 Wide-angle X-ray diffraction patterns of hydrostatically extruded polyethylene. Temperature of extrusion, T_E = 20°C, extrusion ratio, R'_E = 4.8, (a) before annealing, (b) after annealing at 100°C. Extrusion direction: vertical.

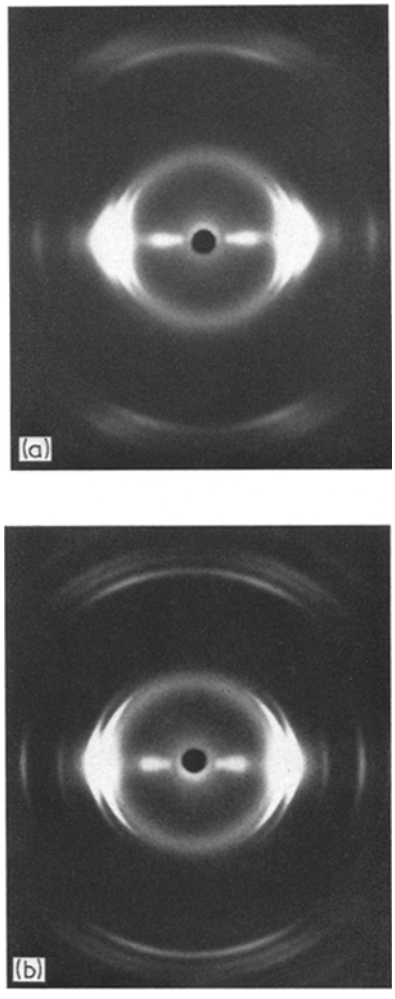

Figure 4 Wide-angle X-ray diffraction patterns of extruded polyethylene. T_E = 20°C, R'_E = 6.4, (a) before annealing, (b) after annealing at 100°C.

illustrated the X-ray diffraction patterns of polyethylene extruded at 20°C with an extrusion ratio of R'_E = 4.8 (R_E = 3.7_4) and 6.4 (R_E = 5.6_7), respectively. The diffraction spots, (110) and (200), of the specimens seem very diffuse. There may be weak spots due to a second form in addition to the spots due to the usual orthorhombic form. As the weak spots disappeared on heating at 100°C, (110) and (200) planes are clearly separate (Figs. 3b and 4b).

To clarify the existence of the (*hkl*) planes of a second form, diagonal scans were made at different azimuthal angles between the meridian (ϕ = 0°) and the equator (ϕ = 90°). As can be seen in Fig. 5, reflections at Bragg angles (2θ), about 19.4, 23.0 and 24.9° were observed for the specimen, R'_E = 4.8. According to the unit cell dimensions and crystal structure of a monoclinic form given by Seto *et al.* [17], these planes correspond to *m*(001), *m*(200) and *m*(20$\bar{1}$), respectively. The innermost peak, *m*(001), was clearly observed at ϕ = 70°. Also, the diagonal scans for the extrudate, R'_E = 6.4, show the *m*(001) diffraction. The partial transformation to a second form is the usual result of cold-working polyethylene. It is seen that besides the stretching [18], rolling [6] and compression [17] of polyethylene, hydrostatic extrusion at room

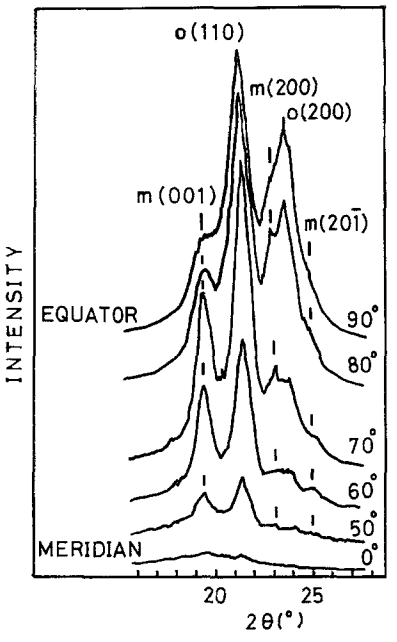

Figure 5 Diagonal scans of extrudate obtained at T_E = 20°C for R'_E = 4.8. The angles in the figure indicate the azimuthal angle (ϕ), meridian: ϕ = 0°, equator: ϕ = 90°. o: orthorhombic phase, m: monoclinic phase.

temperature generates the phase transformation to monoclinic.

3.2. Wide- and small-angle X-ray diffraction patterns

3.2.1. Extrusion ratio, R'_E = 3.0

The wide- and small-angle X-ray diffraction patterns obtained for the specimens extruded at the extrusion ratio R'_E = 3.0 in the temperature range from 20 to 110°C (Fig. 6). In these photographs the extrusion direction of the specimen is vertical. At a first glance, the monoclinic form was not observable. However, the photograph of the specimen extruded at 20°C shows weak *m*(001) spots, which have off-equator maxima.

The wide-angle X-ray diffraction photograph shows shallow off-equator maxima on the (110) ring and equatorial maximum on the (200) ring. It appears that at extrusion ratio, R'_E = 3.0, the *a*-axis of orthorhombic unit cell tends to preferentially line up perpendicular to the extrusion direction. Although in these photographs the (020) diffraction at Bragg angle (2θ), $\sim$ 36.4°, cannot be seen because of its weak intensity, the azimuthal scans show that the intensity distribution of the (020) plane has the off-equator maximum. The *b*-axis lines up at about 29 to 30° off the perpendicular to the direction of extrusion. The (002) plane at Bragg angle (2θ), $\sim$ 74°, has the off-meridian maxima. The *c*-axis lines up at 26 to 32° off the extrusion direction.

The small-angle X-ray scattering pattern of the starting material consisted of a ring having an isotropic intensity distribution and the long period, *L*, $\sim$ 220 Å. Small-angle X-ray photographs of the extruded products at R'_E = 3.0 showed diagrams with four distinct intensity maxima. Besides these four maxima, a two-point pattern on the meridian was observable by close inspection of the original negative. The two-point pattern consists of two faint lines perpendicular to the meridian. It seems that the new fibre structure begins to appear at an extrusion ratio as low as R'_E = 3.0. The six-point pattern is of interest in connection with the deformation mechanism of spherulitic structure. Recently, McConkey *et al.* studied the structural changes of low density polyethylene and reported a six-point small-angle pattern [19].

At low extrusion temperatures, the four maxima align so as to constitute an ellipse having the long axis on the equator. At high extrusion temperatures, the four maxima become parallel to the equator. Here, they are connected through the diffuse scattering around the beam stop. The two-point pattern on the meridian increases in intensity with increasing temperature of extrusion. A more detailed analysis of the deformation process due to hydrostatic extrusion will be reported in the near future.

3.2.2. R'_E = 4.8

Fig. 7 shows some of the wide- and small-angle X-ray diffraction patterns obtained for the specimens extruded at R'_E = 4.8. Although the (200) and (020) diffractions of the orthorhombic phase have wide intensity distributions along the azimuthal angle, they exhibited maxima on the equator. The *b*-axis, as well as the *a*-axis, lined up perpendicular to the extrusion direction. It is seen, therefore, that the *c*-axis (i.e. molecular chain axis) oriented to the extrusion direction. The degree of orientation was not as high as required, since the (200) and (020) spots had intensity distributions.

As shown in Section 3.1, *m*(001), *m*(200) and *m*(20$\bar{1}$) of the monoclinic phase were observed for the specimen extruded at 20°C (R'_E = 4.8). Photographs of specimens extruded at temperatures up to 70°C show diffraction spots due to a

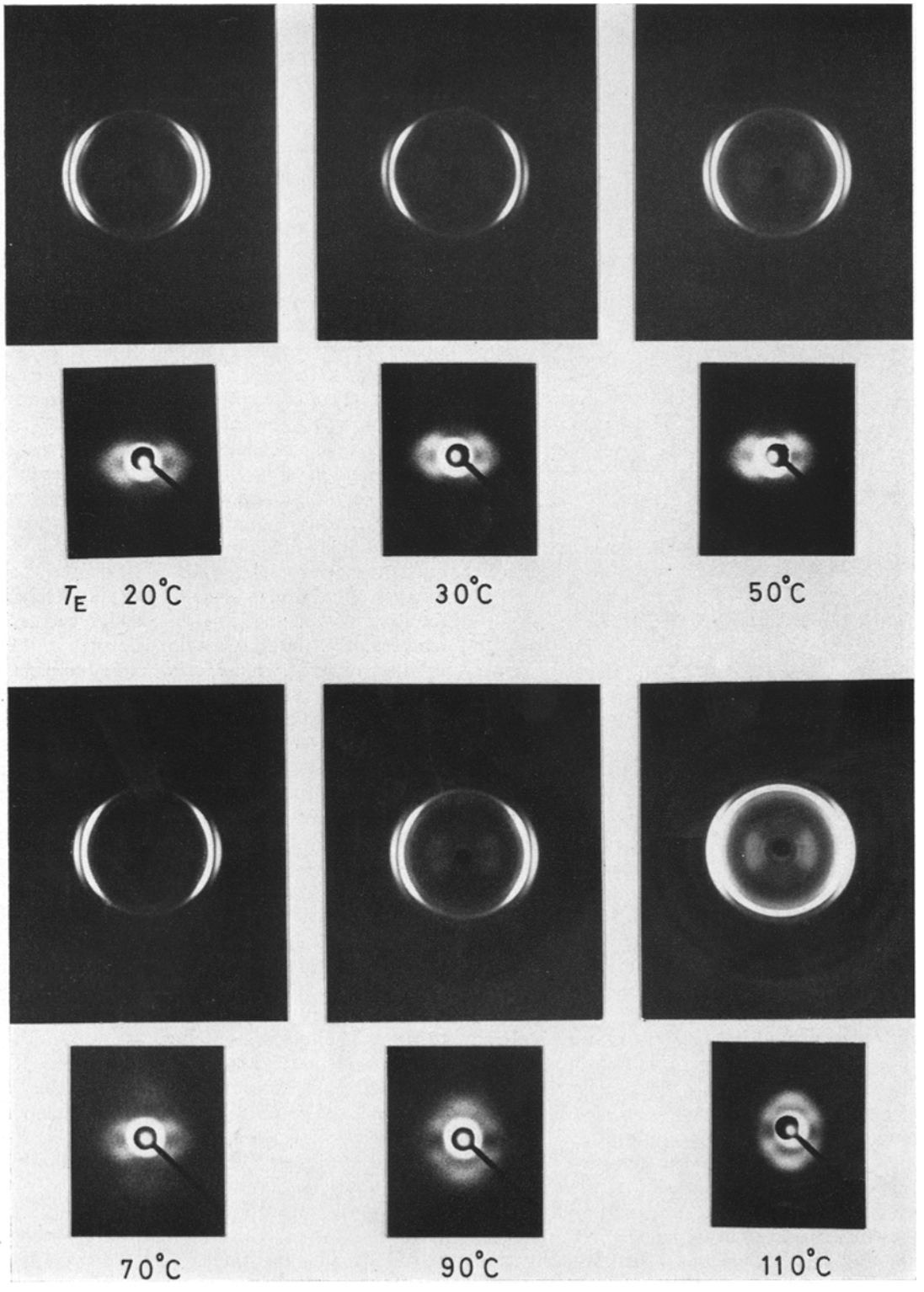

Figure 6 Wide- and small-angle X-ray diffraction patterns of extrudates for $R'_E = 3.0$. $T_E = 20$ to 110°C.

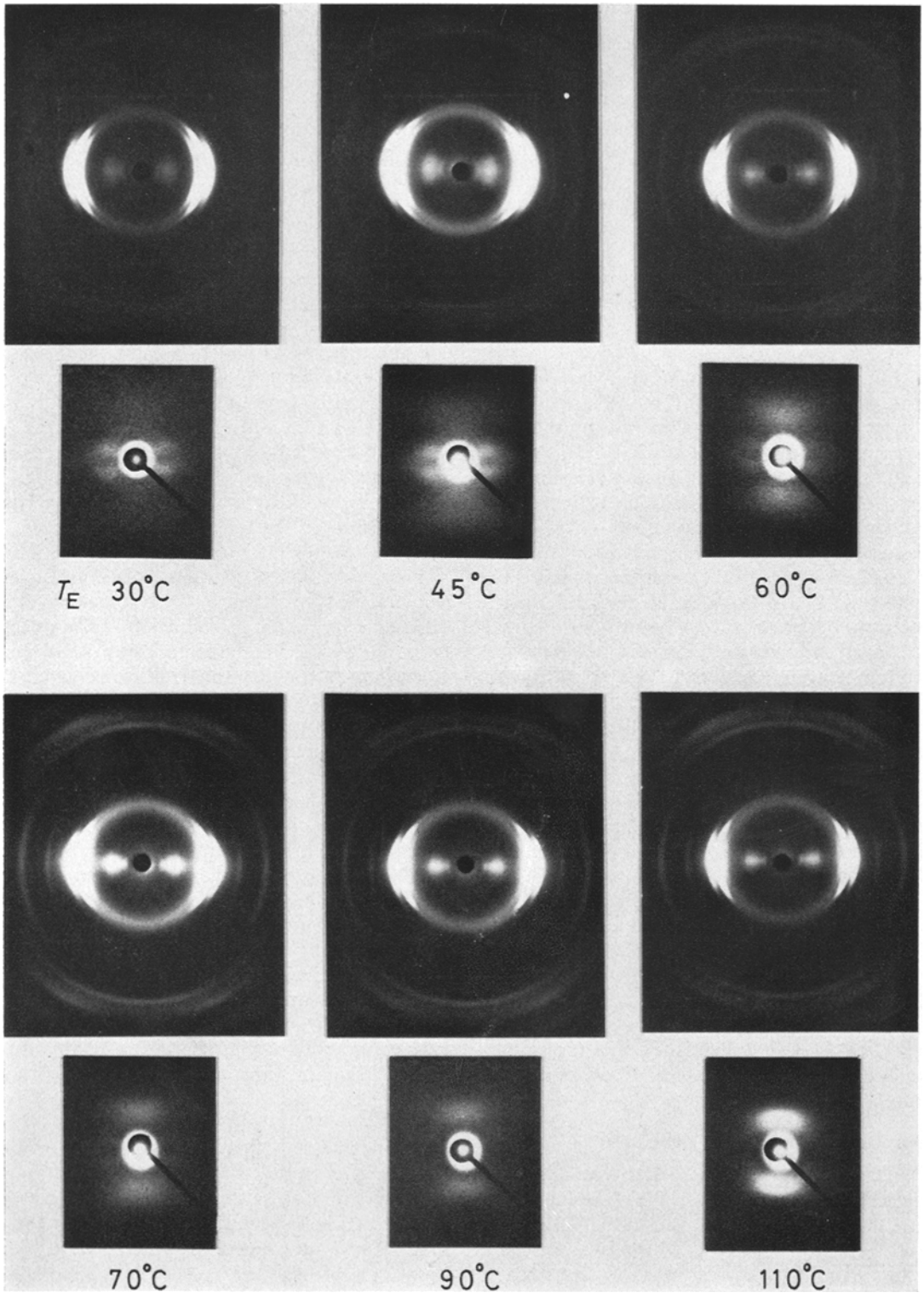

Figure 7 Wide- and small-angle X-ray diffraction patterns of extrudates for $R'_E = 4.8$. $T_E = 30$ to 110°C.

monoclinic phase. At a higher extrusion temperature (e.g. 80°C), the spot of monoclinic phase is hardly discernible.

Small-angle X-ray scattering photographs of the specimens, extruded at $R'_E = 4.8$ in the temperature range up to 70°C, showed diagrams with four distinct intensity maxima parallel to the equator and with two intensity maxima on the meridian. The extruded products at the temperature 80 to 110°C gave only the two-point diagram elongated perpendicular to the meridian. The intensity maxima increase in intensity with increase in temperature of extrusion.

3.2.3. $R'_E = 6.4$

In Fig. 8, the wide-angle X-ray diffraction photograph shows clearly the *c*-axis orientation pattern known as a "fibre diagram". The paratropic diffractions, (110), (200), (210) and (020) spots, had maxima on the equator. It is seen that the *a*- and *b*-axes are aligned perpendicular to the extrusion direction. There was a broad halo present at Bragg angle $(2\theta) \sim 19.5°$, which corresponds to the amorphous phase. The monoclinic phase was clearly observed for the specimen obtained at low extrusion temperature. Even the specimen obtained at high extrusion temperature seems to have a small fraction of monoclinic phase, because in the X-ray photograph the (200) and (210) spots are not clearly separated.

Small-angle X-ray scattering photographs of the specimens, extruded at $R'_E = 6.4$ in the temperature range up to 50°C, showed diagrams with intensity maxima on the meridian and in addition faint lines on the equator were observed. As the temperature of extrusion increases, the two-point pattern on the meridian increases in intensity. At first glance, the pattern at low extrusion temperature ($T_E = 30°C$) appears to consist of two intensity maxima elongated perpendicular to the meridian. However, close inspection of the original negative indicates a diagonal four-point pattern (X-shaped scattering).

3.2.4. $R'_E = 9.0$

In Fig. 9 the *a*- and *b*-axes are well aligned transversely, indicating high chain orientation. It must first be stipulated that the equatorial streaks due to the presence of "voids" elongated in the direction of extrusion are not observable in the small-angle X-ray scattering photographs. As the photographs show two intensity maxima elongated perpendicular to the meridian (i.e. a line-shaped two-point pattern), it is seen that the lateral dimensions of the crystallites are small. The scattering intensity decreases with increasing extrusion ratio. Wide- and small-angle X-ray diffraction patterns show the highly-oriented fibre structure in which stacks of folded chain crystallite are present.

3.3. Long period

The axial long period, indicative of a periodic structure in these hydrostatically-extruded specimens, was calculated from meridional maxima of small-angle X-ray scattering. In Fig. 10 the axial long period, L, was plotted against the temperature of extrusion, T_E, which varied from 20 to 110°C. At low temperature (e.g. 20 to 50°C), L increases with increasing extrusion ratio, R'_E. At temperatures higher than 80°C, L decreases with increasing R'_E and increases with increasing T_E. There is a conspicuous influence of temperature of extrusion on the long period. At $50 < T_E < 70°C$, L drastically changes.

The hydrostatic extrusion of polyethylene shows some similarities, but also some important differences from the stretching of polyethylene in respect to small-angle X-ray scattering. Corneliussen and Peterlin [20] investigated the effect of drawing temperature on the deformation of polyethylene. They observed that the long period first increased rather slowly with temperature and finally increases rapidly near the melting point. Upon drawing, the final meridional long period in the highly drawn portions are independent of the draw ratio [7]. On the other hand, in the case of hydrostatic extrusion the long period exhibits complex variations as shown in Fig. 10. Moreover, at temperatures above 70°C, the long period decreases slightly with increasing extrusion ratio (R'_E). Strictly speaking, the intensity distribution of small-angle scattering should be considered carefully. However, the long period data in Fig. 10 were calculated from the scattering maxima according to Bragg's law.

3.4. Degree of crystalline orientation

The wide-angle X-ray photographs of the specimens at high extrusion ratio exhibit typical *c*-axis orientation patterns. It is apparent that high molecular orientation occurs during extrusion. In order to characterize better the *a*, *b*- and *c*-axis state of orientation, the azimuthal scannings of (200) and (020) reflections were carried out. The degree of orientation for these axes, f_a,

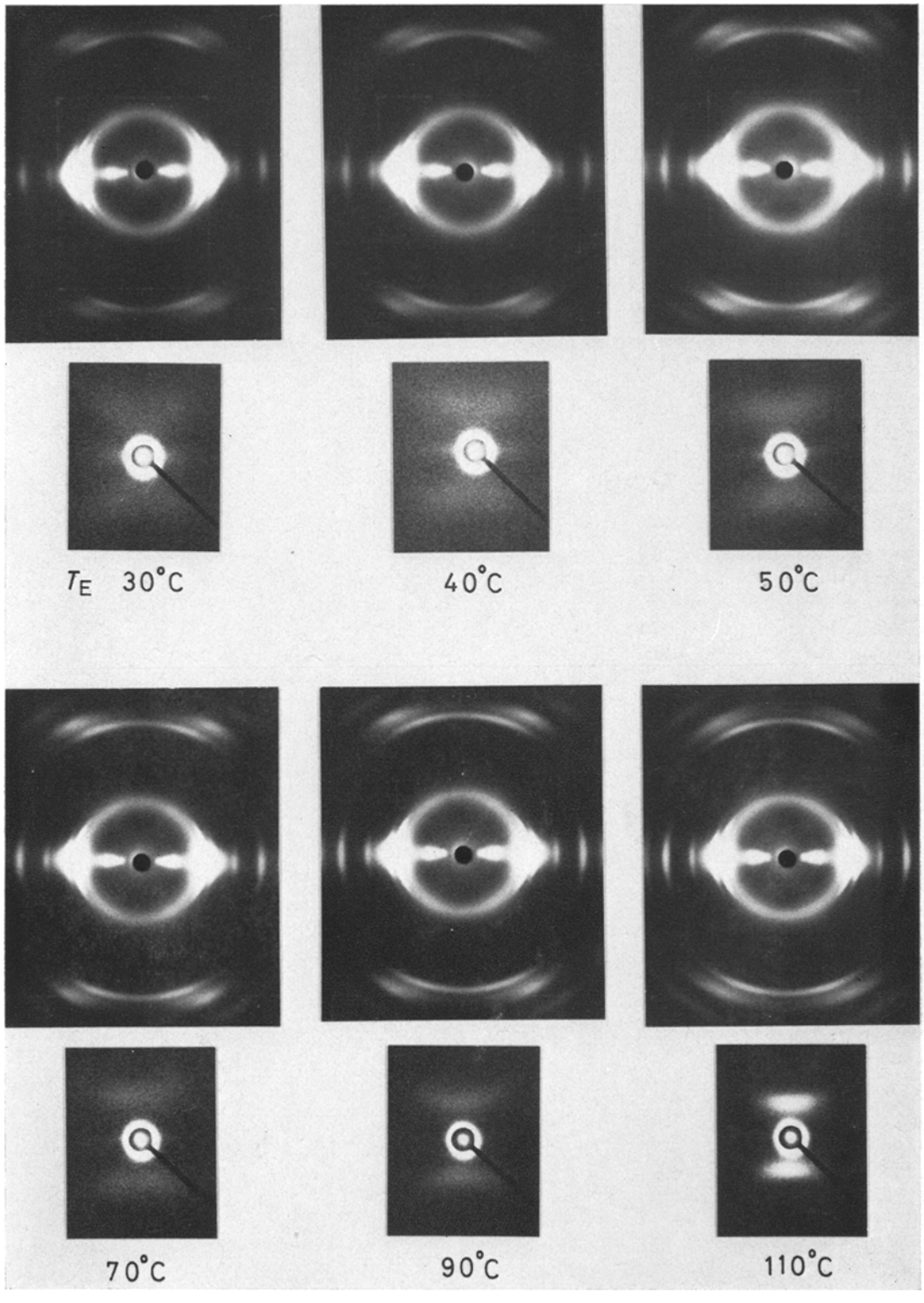

Figure 8 Wide- and small-angle X-ray diffraction patterns of extrudates for $R'_E = 6.4$. $T_E = 30$ to 110°C.

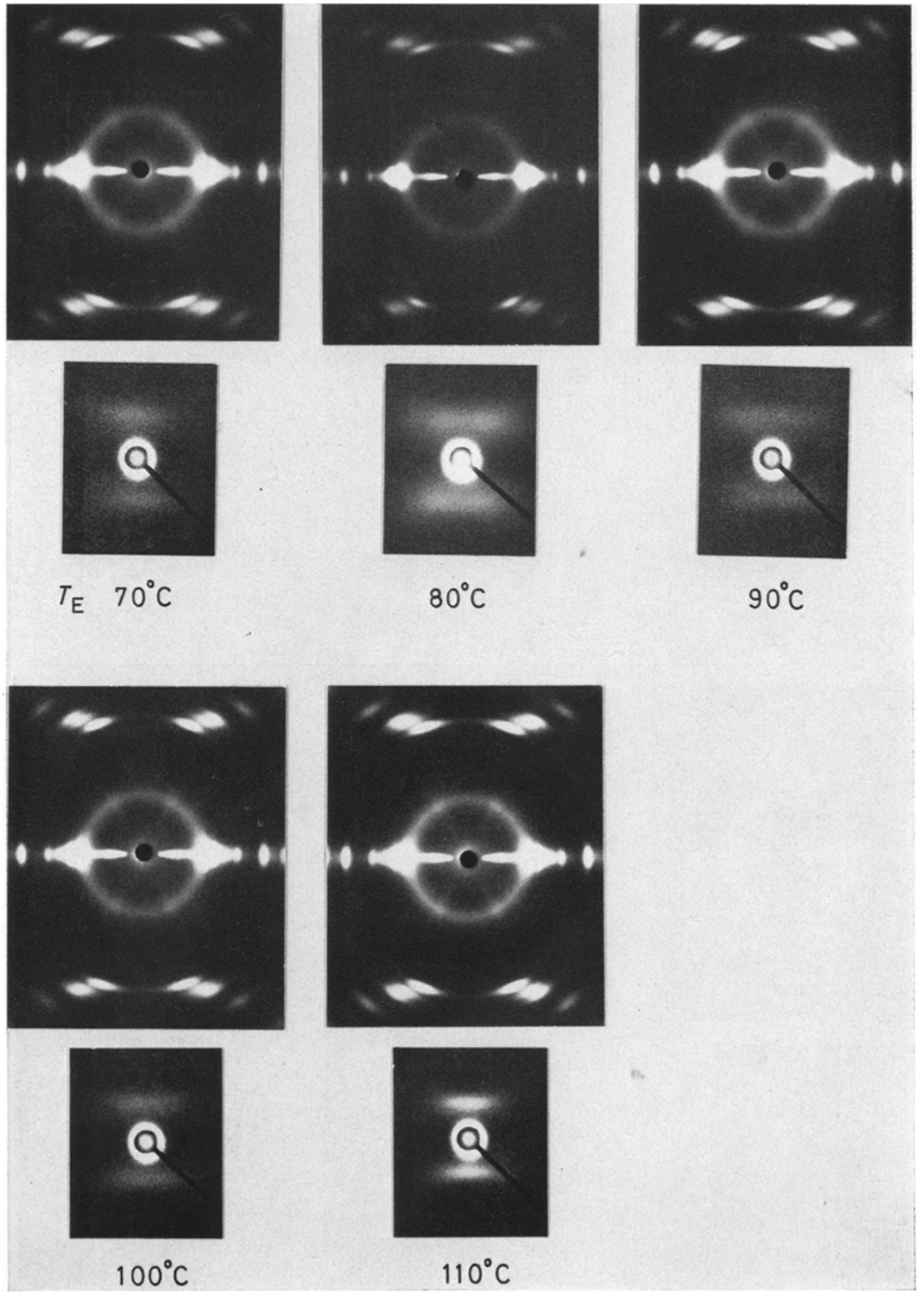

Figure 9 Wide- and small-angle X-ray diffraction patterns of extrudates for $R'_E = 9.0$. $T_E = 70$ to 110°C.

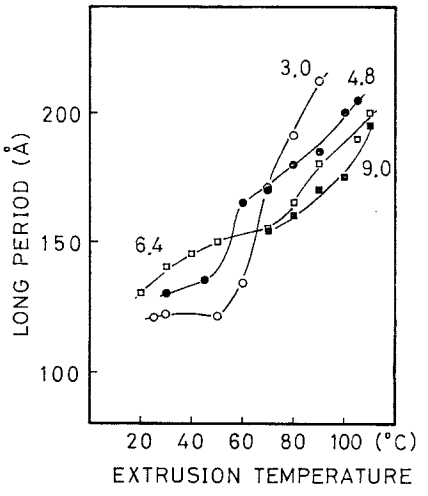

Figure 10 Axial long period (L) calculated from the meridional maxima of small-angle X-ray scattering versus temperature of extrusion (T_E). Extrusion ratio (R'_E), ○: 3.0, ●: 4.8, □: 6.4, ■: 9.0.

f_b and f_c, were calculated using Equations 1 to 3.

In Fig. 11, the degree of orientation of the orthorhombic phase was plotted against the extrusion ratio, R_E. At $R_E \geqslant 6$, there is little difference between the a- and b-axes from the viewpoint of orientation. Moreover, the chain axis of polyethylene aligns to the extrusion direction. Imada *et al.* [8] studied the solid-state extrusion of polyethylene and concluded that the extrudates at 110°C with the degree of processing (i.e. extrusion ratio) 16 showed the highest c-axis orientation.

At low extrusion ratios, the orientation of the a-axis is noticeably different from that of the b-axis. The a-axis tends to align preferentially perpendicular to the extrusion direction. It has been shown by Stein [16] that the a-axis orients at first more readily than does the b-axis during stretching of polyethylene. It seems that the stretching and the hydrostatic extrusion have much in common with respect to the orientation and the deformation behaviour of polyethylene.

The degree of c-axis orientation (f_c) at high extrusion ratios ($R'_E = 9.0$) does not change with the temperature of extrusion (T_E); at $R'_E = 3.0$ and 6.4, f_c, in general, increases with an increase in T_E. However, at $R'_E = 3.0$, f_c at 110°C is slightly lower than at 90°C. It seems that partial melting occurred during extrusion at such a high temperature. In addition, recrystallization and relaxation of the amorphous region also occurs immediately after the polymer has been extruded through the die.

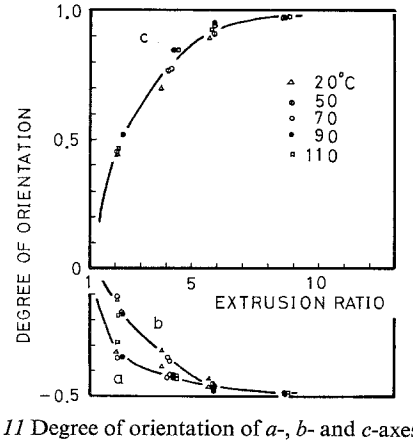

Figure 11 Degree of orientation of a-, b- and c-axes versus extrusion ratio. Temperature of extrusion (T_E), △: 20°C, ⓘ: 50°C, ○: 70°C, ●: 90°C, □: 110°C.

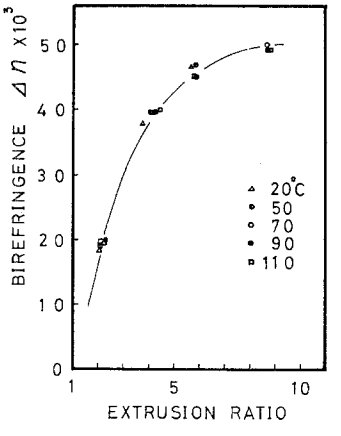

Figure 12 Birefringence of extrudates versus extrusion ratio. T_E = 20 to 110°C.

3.5. Birefringence (Δn) and degree of amorphous orientation

The variation of Δn with extrusion ratio is plotted in Fig. 12. The birefringence increases monotonically with extrusion ratio, but at high extrusion ratios it begins to approach a limiting value. On the other hand, the birefringence does not change dramatically with the temperature of extrusion.

The amorphous orientation of stretched polyethylene had been determined assuming the additivity of the birefringence contributions of the crystalline phase and the amorphous phase [15]. If one assumes that the hydrostatically-

extruded polyethylene is a two-phase mixture containing an amorphous region and crystallites, the total birefringence, Δn, can be written as in Equation 6. Here, the contribution of "form birefringence" [21] is nglected.

By substituting the values of f_c, X_v and Δn into Equations 6 to 8, the amorphous orientation (f_{am}) was obtained. The variation of f_{am} with the extrusion ratio (R_E) was plotted in Fig. 13. The amorphous orientation increases rapidly with increasing extrusion ratio. Moreover, the amorphous orientation changes strongly with the temperature of extrusion. The molecular orientation of amorphous region produced at a given extrusion ratio is greater for extruding at lower temperatures than at higher ones.

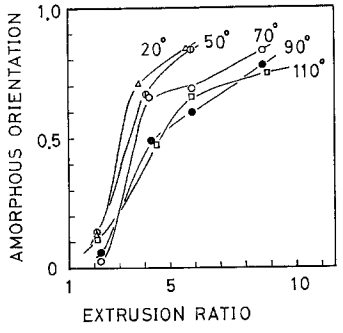

Figure 13 Variation of amorphous orientation with extrusion ratio. The temperatures of extrusion (T_E) are indicated in the figure.

It is important to recognize that the procedure used to determine the amorphous orientation (f_{am}) by using f_c, X_v and Δn has several limitations. First, the uncertainty of the value of $\Delta n_{am}{}^{o}$ must be recognized. This, however, does not prevent the use of Equation 6. By using different values of $\Delta n_{am}{}^{o}$, a small change in the calculated value of f_{am} was found but there was no change in the general situation. Secondly, the possibility of form birefringence is ignored. A third limitation is that the formula for crystallinity is based upon the assumption that the density of the amorphous region (d_a) in Equation 4 is not affected by mechanical treatment. This is not strictly true for the highly extended amorphous region. Statton [22] has pointed out that crystallinity is dependent on the method of measurement. The actual value of d_a may be somewhat higher than the value used here for d_a (i.e. 0.855 g cm^{-3}). The experimental values of X_v given here, therefore, may be higher than the actual value. A fourth limitation is that the existence of the monoclinic phase, especially in the specimen extruded at lower extrusion temperature, was neglected: Equation 6 is based upon the simplified assumption that the hydrostatically-extruded polyethylene is a two-phase mixture containing crystalline and amorphous regions. For these reasons, the molecular orientation of amorphous region shown in Fig. 13 should be regarded as approximate. However, the influence of R'_E and T_E on f_{am}, mentioned above, is expected to be reasonable.

3.6. Structure-feature relationship

As already mentioned, products obtained by the steady-state hydrostatic extrusion have smooth surfaces, especially those produced at a high extrusion ratio. The significant feature of specimens produced at high extrusion ratios is their high degree of transparency. The starting material and extrudates for R'_E = 3.0 and 4.8, were opaque whereas extrudates for R'_E = 6.4, which showed c-axis orientation, were translucent. Extrudates for R'_E = 9.0, which showed highly oriented typical fibre diagram, were highly transparent.

Recently, transparent high-density polyethylene has been prepared by means of various special techniques. Southern and Porter [23] obtained a transparent polyethylene filament in a capillary rheometer under certain conditions of combined strain and pressure. Wang *et al.* [24] described a quench-rolling process by which a highly transparent polyethylene film could be produced. Furthermore, Krueger and Yeh [25] reported that transparent polyethylene had been prepared by shearing molten polyethylene between two concentric cylinders. Since the procedures conducted by these authors involve shearing processes, it can be seen that the process for preparing transparent polyethylene consists of a "strain-induced" crystallization. Kitamaru *et al.* [26] studied the crystallization of a lightly cross-linked polyethylene in which molecular chains were elastically deformed by compression. They determined the conditions that induce transparent films and discussed the origin of the transparency as resulting from a particular orientation of the crystalline phase.

In all the works mentioned above [23-26] there is a common process, i.e. crystallization from the melt under a certain strain. On the other hand, Imada *et al.* [8] obtained a transparent product by

plastic deformation of polyethylene: solid polymer was extruded through a tapered die at a temperature higher than 80°C but below the melting point. Our experiments on the hydrostatic extrusion of solid polyethylene bear a close resemblance to those conducted by Imada *et al.* on the direct extrusion in this respect.

In order to give an explanation of the transparency of our products, it is necessary to look at the crystalline state and the supermolecular structure. The extrudate for a high extrusion ratio ($R'_E = 9.0$) shows a high degree of *c*-axis orientation. The amorphous chain, also, is oriented pretty well to the extrusion direction and the extrudate was easily cut in the direction parallel to the extrusion direction with a razor blade. Furthermore, when struck with a hammer, a fibrous type of fracture was produced. The small-angle X-ray scattering photographs of the specimen extruded at high extrusion ratio, showed a line-shaped two-point pattern (Fig. 9). The lateral dimensions of the crystallites may be small as can be deduced from the lateral width of the meridional maxima. Therefore, it is convenient to imagine the structure of extrudate as a highly oriented fibre structure which is closely filled with fully oriented crystallites; a model of the basic element of the fibre structure was developed by Peterlin [27] on the basis of deformational studies of polyethylene. Between the microfibrils, highly extended amorphous chains may exist. The degree of crystallinity of extrudate for $R'_E = 9.0$ being in the range of $62 \sim 66\%$, there should be a fairly large amount of interfibrillar amorphous chain bundles. The outstanding properties of our products, i.e. transparency and fibrosity, can be accounted for by a typical fibre structure in which few remarkable "voids" exist.

4. Summary and conclusions

The previous papers of this series dealt with the extruding conditions of solid polyethylene; the present paper has characterized the molecular orientation of extrudates and the structural changes of polyethylene in hydrostatic extrusion. As the extrudates obtained by the steady-state hydrostatic extrusion have a homogeneous cross-section along their length, it is possible to develop a fundamental understanding of the effects of the extrusion ratio and extrusion temperature on the molecular orientation of the crystalline and amorphous regions of polyethylene. The results and conclusions of this study can be summarized as follows:

(1) The hydrostatic extrusion of solid polyethylene at low temperatures (especially at room temperature) generates a partial transformation from the orthorhombic to the monoclinic phase;

(2) The small-angle X-ray scattering patterns for low extrusion ratios show diagrams with six intensity maxima, which consists of four point quadrant maxima and two point meridional maxima;

(3) The small-angle X-ray scattering patterns for high extrusion ratios show diagrams with two intensity maxima elongated perpendicular to the meridian;

(4) The *a*-axis tends to line up perpendicular to extrusion direction in preference to the *b*-axis;

(5) At extrusion ratio (R_E) $\geqslant 6$ the chain axis of polyethylene aligns with the extrusion direction. Wide- and small-angle X-ray diffraction patterns show the highly oriented fibre structure;

(6) As the extrusion temperature rises, it seems that the polyethylene rods become more susceptible to plastic deformation through crystalline orientation. At high temperatures, the destruction of the original lamellae and the rotation of the folded chain blocks are prominent;

(7) The birefringence of the extrudate increases monotonically with the extrusion ratio;

(8) The orientation of the amorphous chain increases with increasing extrusion ratio and decreases with increasing extrusion temperature;

(9) The outstanding properties of the extrudate can be accounted for by a typical fibre structure.

The hydrostatic extrusion and stretching have much in common with the orientation and deformation behaviour of polyethylene. However, hydrostatic extrusion shows some difference from the latter in respect of the small-angle X-ray scattering. Further study is required to clarify the mechanism of deformation during extrusion.

References

1. H.LL. D. PUGH and A. H. LOW, *J. Inst. Metals* **93** (1964-65) 201.
2. A. BUCKLEY and H. A. LONG, *Polymer Eng. Sci.* **9** (1969) 115.
3. J. M. ALEXANDER and P. J. M. WORMELL, *Ann. C.I.R.P.* **19** (1971) 21.
4. M. HORIO, *J. Soc. Rheology, Japan* **1** (1973) 28.
5. T. WILLIAMS, *J. Mater. Sci.* **8** (1973) 59.
6. I. L. HAY and A. KELLER, *ibid* **1** (1966) 41.

7. G. MEINEL, N. MOROSOFF and A. PETERLIN, *J. Polymer Sci. A-2* **8** (1970) 1723.
8. K. IMADA, T. YAMAMOTO, K. SHIGEMATSU and M. TAKAYANAGI, *J. Mater. Sci.* **6** (1971) 537.
9. K. NAKAYAMA and H. KANETSUNA, *Kobunshi Kagaku* **30** (1973) 713.
10. *Idem, ibid,* **31** (1974) 256.
11. *Idem, ibid,* **31** (1974) 321.
12. Z. ZIMERMAN and B. AVITZUR, *Trans. ASME* **92** *Series B* (1970) 119.
13. P. H. HERMANS, "Physics and Chemistry of Cellulose Fibres" (Elsevier, Amsterdam, 1949).
14. M. G. GUBLER and A. KOVACS, *J. Polymer Sci.* **34** (1959) 551.
15. R. S. STEIN and F. H. NORRIS, *ibid* **21** (1956) 381.
16. R. S. STEIN, *ibid* **34** (1959) 709.
17. T. SETO, T. HARA and K. TANAKA, *Jap. J. Appl. Phys.* **7** (1968) 31.
18. E. R. WALTER and F. P. READING, *J. Polymer Sci.* **21** (1956) 557.
19. B. H. MCCONKEY, M. W. DARLINGTON, D. W. SAUNDERS and C. G. CANNON, *J. Mater. Sci.* **6** (1971) 572.
20. R. CORNELIUSSEN and A. PETERLIN, *Macromol. Chem.* **105** (1967) 193.
21. F. A. BETTELHEM and R. S. STEIN, *J. Polymer Sci.* **27** (1958) 567.
22. W. O. STATTON, *ibid* **C18** (1967) 33.
23. J. H. SOUTHERN and R. S. PORTER, *J. Macromol. Sci. Phys.* **4** (1970) 541.
24. T. T. WANG, H. S. CHEN and T. K. KWEI, *J. Polymer Sci.* **B8** (1970) 505.
25. D. KRUEGER and G. S. Y. YEH, *J. Appl. Phys.* **43** (1972) 4339.
26. R. KITAMARU, H.-D. CHU and S.-H. HYON, *Macromolecules* **6** (1973) 337.
27. A. PETERLIN, *J. Polymer Sci.* **C18** (1967) 123.

Received 18 September and accepted 31 December 1974.